

AD-A102 254

NATIONAL BUREAU OF STANDARDS WASHINGTON DC  
LASER ABLATION AND RESONANCE IONIZATION SPECTROSCOPY (LARIS) FO-ETC(U)  
1980 S MAYO, T B LUCATORTO, G G LUTHER N00014-80-F-0046  
NL

UNCLASSIFIED

1 of 1  
AD-A102 254

END  
DATE  
FILED  
8-81  
DTIC

22  
24  
10  
1  
AD A102234

Laser Ablation and Resonance Ionization Spectroscopy (LARIS)  
for Trace Analysis of Solids

LEVEL II

10  
S. Mayo, Center for Electronics and Electrical Engineering,

T. B. Lucatorto, Center for Radiation Research,

and

G. G. Luther, Center for Absolute Physical Quantities

Q1725  
Q210  
DTIC  
ELECTE  
S JUL 30 1981  
D  
E

National Bureau of Standards

Washington, DC 20234

ADVANCE COPY,  
FOR REVIEW ONLY

\*This work, conducted as part of the Semiconductor Technology Program at the  
National Bureau of Standards, was supported in part by the Office of Naval  
Research, Order No. 15 N00014-80-F-0046. Not subject to copyright.

DISTRIBUTION STATEMENT A

Approved for public release;  
Distribution Unlimited

81 7 29 040  
110680

DTIC FILE # 700V

Key Words

laser ablation  
laser-produced vaporization  
laser-solid interaction  
plasma production and heating by laser beam  
pulsed-dye laser application  
resonance ionization spectroscopy  
trace analysis of solids  
two-photon absorption spectroscopy

Accession For	
NTIS GRA&I	<input checked="" type="checkbox"/>
DTIC TAB	<input type="checkbox"/>
Uncontrolled	<input type="checkbox"/>
Journal citation	<input type="checkbox"/>
<i>See on file</i>	
By _____	
Distribution/	
Availability Codes	
Dist	Avail and/or Special
A	

Abstract

A new analytical technique has been developed for the detection of trace sodium impurity in single crystal silicon using laser ablation and resonance ionization spectroscopy. Sodium is detected in the ablated vapor by using two tunable laser probes to induce resonantly enhanced multiphoton ionization via the intermediate 3P and 4D levels. At present the technique provides only relative quantitative results. For absolute quantitative results, characterization of complex laser-solid interaction phenomena in a buffer gas is required. The minimum detectable sodium density in the solid is estimated to be about  $10^{11}$  atoms/cm<sup>3</sup>. Generalization of this technique to other impurities is limited only by laser availability. -

I. Introduction

The need for developing highly sensitive analytical techniques springs from the continuous demand for the higher purity materials required to understand fundamental properties and explore new engineering applications.

Semiconductors used for electron device fabrication offer a prominent example of such materials because their electrical properties may be influenced by minute amounts of donor or acceptor impurities. The highest sensitivity required to characterize such pure materials is determined by the minimum dopant density in the solid capable of producing measurable electrical effects. Clearly, for dopants controlling the bulk resistivity, this limit is set by the carrier density in the intrinsic semiconductor since below this limit no measurable effects associated with impurities in the solid can be observed electrically. For example, at room temperature the intrinsic carrier number densities in germanium, silicon, and gallium arsenide are, respectively,  $10^{13}$ ,  $10^{10}$ , and  $10^7 \text{ cm}^{-3}$  (1). Characterization of such materials would demand analytical sensitivities as high as one part in  $10^{10}$ ,  $10^{13}$ , and  $10^{16}$ , respectively, a rather formidable task.

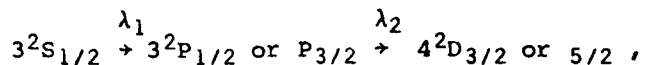
Recently, single-atom detection in gases has been demonstrated by resonance ionization spectroscopy (RIS) on a variety of atomic species (2). A single cesium atom was detected in an environment of  $10^{19}$  atoms or molecules of another gaseous species (3), and a similar result was reported on lithium (4). The technique consists of selective multiple-photon absorption by the atom followed by photoionization and detection of the ejected electron. The RIS scheme used to identify a particular species is determined by the

spectroscopic structure of the atom and the availability of lasers to match the atomic transition lines. A variety of such schemes has been proposed for a number of elements (2). Another highly selective single-atom detection technique similar to RIS has also been demonstrated; this technique involves laser excitation of high energy Rydberg states followed by electric field ionization of the atom (5-7). Incorporation of RIS in a new scheme for analysis of solids may help to develop the high analytical sensitivities required to characterize pure semiconductor materials.

Single-atom detection capability offers an extraordinary opportunity to develop a high-sensitivity analytical technique for solids. Laser ablation under controlled atmosphere can be used to evaporate a small amount of homogeneous materials. The evaporated plume reaches thermal equilibrium with the atmosphere forming a gas sample appropriate for RIS analysis. We call this technique LARIS, or laser ablation and resonance ionization spectroscopy. An evaluation of LARIS was made to demonstrate its applicability as an analytical technique to measure trace sodium contamination in semiconductor materials. Sodium was selected because its spectroscopic structure allows the use of simple laser technology.

## II. Single Atom Detection Apparatus

An RIS-sodium detection apparatus was first built as part of the LARIS instrumentation. The RIS scheme used involves photons with two different wavelengths (2). Sodium can be photoionized from the 4D level via the resonance transitions:



where wavelengths  $\lambda_1 = 589.6$  nm or  $589.0$  nm and  $\lambda_2 = 568.8$  nm or  $568.2$  nm can be used. We used the  $\lambda_1$ -blue plus the  $\lambda_2$ -red combination. However, since this process takes place in a buffer gas atmosphere, collisional level mixing is expected (8), and consequently the 4D-level population is independent of which wavelength combination is used. Photoionization from the 4D-level may be produced by either color.

The apparatus consists of a cylindrical gold-plated brass chamber 10.16 cm outer diameter, 8.89 cm in inner diameter, and 15.2 cm long provided with off-center laser collimators containing multiple circular apertures and a cone-shaped aperture spaced inside an 11-cm long tube holding the windows (see Fig. 1). The collimators are made of chemically treated brass to provide a black nonreflective surface. A small oven containing metallic sodium is attached to the chamber, allowing the evaporation of controlled amounts of sodium.

A proportional counter was built inside the chamber. The anode is a stainless steel wire 50  $\mu\text{m}$  in diameter shielded at each end by a coaxial field tube. The field tubes were held at the potential appropriate for zero field distortion. They determine the counter active length and serve to trap the photoelectrons ejected from the windows by the lasers. The counter was operated with flowing high-purity P-10 gas (90-percent argon plus 10-percent methane) at a pressure of about 126 kPa (95 Torr). The total water and oxygen impurities in the gas were less than 1 ppm (9).

The cathode is a cylindrical grid mounted on insulation rings 7.3 cm in diameter placed inside the counter (10). The grid is made of 120 nickel wire (127- $\mu$ m diameter) straight sectors parallel to the counter wall, equally spaced around the rings. The grid is kept negative with respect to the wall, so the actual counter electric field is established between the central anode wire and the grid.

The grid is used to suppress photoelectrons ejected from the counter wall by the scattered light background; even a monolayer of sodium coverage on the wall reduces the metal work function, allowing electron emission for the RIS-wavelengths used. The suppression effect of the grid was tested by measuring the number of single electrons ejected from the wall by a uv-mercury lamp. A small bias voltage was applied to the grid when the anode potential was +1000 V with respect to the grounded wall. The integrated uv-generated electron spectra was a hundred times smaller with -10 V grid bias, in comparison with similar spectra measured with +10 V grid bias. Occasionally, the grid was cleaned in situ by electrically heating it in vacuum.

Gas multiplication factors (11) in the  $10^3$ -range were used to check single electron detection capability (12,13). A charge-sensitive preamplifier attached to the anode was used to measure the avalanche current. The charge-to-voltage conversion factor was 1 microvolt per collected electron.

The counter linearity was checked up to 300 primary electrons by using the  $^{55}\text{Fe}$  x-ray (5.9 keV) plus x-ray fluorescence induced by  $^{109}\text{Cd}$  x-ray (22 keV) on titanium (4.5 keV), iron (6.4 keV), nickel (7.48 keV), and copper (8.05 keV). The argon escape peak associated with each x-ray peak was used for calibration down to about 55 primary electrons.

The probes are pulsed coaxial flashlamp-pumped dye lasers with quadraxial adapters for high pulse stability and low beam divergence (14). Each laser beam was passed through a 3:1 reducing telescope provided with a spatial filter. The beam diameter inside the counter was about 0.3 cm. Since the counter active length is about 5 cm, the total active volume (where RIS-generated electrons can be detected) is about  $0.4 \text{ cm}^3$ . The laser wavelength was tuned by an intracavity dispersive system formed by three 60-deg (Schott SF-10) glass prisms. A small fraction of each laser probe was monitored by a spectrograph-optical multichannel analyzer combination with  $25 \mu\text{m}$  resolution. Typical laser energies were 0.3 to 0.5 joule per pulse. The pulse full width at half maximum was about  $0.6 \mu\text{s}$  and the spectral width was 0.07 nm. The pulse-to-pulse energy variation was a few percent (pulse energy measured with a calorimeter).

The single atom ionization probability can be approximated under our experimental conditions as  $1 - \exp(-g\sigma\phi)$  where  $g = g_2/(g_0 + g_1 + g_2)$  is the relative statistical weight of the photoionized level ( $4^2\text{D}$ ),  $g_0$ ,  $g_1$ , and  $g_2$  are statistical weights of the RIS-involved levels,  $\sigma = 1.5 \times 10^{-17} \text{ cm}^2$  is the  $4^2\text{D}$  level photoionization cross section (15), and  $\phi$  is the pulse photon flux. For 0.99 ionization probability, the required photon flux is  $5 \times 10^{17} \text{ cm}^{-2}$ . A sodium signal associated with about  $10 \text{ atoms/cm}^3$  is shown in Fig. 2.

The probe energy was about 0.3 joule per pulse, for a flux of about  $10^{18} \text{ cm}^{-2}$ .

### III. Laser Ablation for Analysis of Solids

Laser ablation has been extensively used for spectroscopic analysis of solids (16-19). Analytical techniques using laser ablation together with atomic emission (20), atomic absorption (21), resonance fluorescence (22), or time-of-flight mass identification (23) have been reported with sensitivities in the ppm and sub-ppm range. The solid is ablated in air or vacuum, and the ejected plume is optically or mass analyzed. Recently, the feasibility of using resonance ionization as a source for mass spectroscopy was reported (24). The use of laser ablation as part of an analytical scheme for solids needs to be carefully studied before it can be used to obtain accurate quantitative information on the composition of the solid. The phenomena that need to be characterized are:

1. the dynamics of the laser-solid interaction from the perspective of impurity redistribution in the specimen;
2. the dynamics of the plume, i.e., the time-dependent density distribution of the ablated material;
3. the irradiance conditions appropriate for creation of craters with easily quantifiable volumes; and
4. the chemical reactivity of the analyzed species with other components in the plume and in the buffer gas.

The object of the present experiments was to demonstrate the high sensitivity of LARIS; the characterization of items 1 to 4 above, needed to accurately quantify the impurity content in the solid, will be the object of future experimental work.

The ablation process for LARIS takes place in the counter atmosphere. The evaporated target material reaches thermal equilibrium with the buffer atmosphere forming a gas sample close to the solid. Several modifications to the counter were made for the ablation experiments. The grid was replaced by a cylindrical cathode 7 cm in diameter provided with apertures to admit the target and the ablation laser as shown in Fig. 3. The grid was not needed in these experiments since the sodium released from the ablated material was not enough for a monolayer coverage. The coaxial RIS probes passed 0.3 cm away from the target. The anode was replaced by a stainless steel wire 13  $\mu$ m in diameter and the electric field reduced to extend the counter linear range up to 2000 primary electrons.

The ablation laser was a pulsed flashlamp-pumped dye laser similar to the RIS probes. Its output had a broad spectral width ( $\pm 2$  nm centered at 590 nm). The pulse energy was up to 0.5 J with 0.6- $\mu$ s pulse duration. The focal spot on the target was 50 to 100  $\mu$ m in diameter.

Figure 4 shows the laser-generated silicon ablation plume in the counter atmosphere. At expanding velocities (estimated about  $10^5$  cm/s), the total scattering cross section for both neutral and ionized sodium in the counter atmosphere (about  $10^{18}$  argon/cm<sup>3</sup>) is high enough ( $10^{-14}$  cm<sup>2</sup>) to provide appropriate stopping power to form the RIS sample (25,26). With a laser

irradiance of about  $5 \times 10^9 \text{ W/cm}^2$ , a glowing region about  $0.1 \text{ cm}^3$  is formed in front of the target; for a fixed irradiance, the size and shape of this region is determined by the gas atmosphere. The actual RIS analysis takes place in the gas in front of the target after a delay time selected to allow thermalization of the plume.

Alkalies react with oxygen and water contamination in the counter gas reducing the atomic species available for RIS analysis. This may lead to erroneous data if the elapsed time after the gaseous sample formed by the ablation is too long. Characterization of these effects requires kinetic reaction data; such data are generally not available. An estimate of the sodium-oxygen interaction in argon at room temperature can be made by comparison with similar data obtained on cesium (2). The cesium number density decays by a factor of one hundred in 0.6 ms in 133 kPa (100 Torr) argon atmosphere containing 100 ppm oxygen. Following the general trend exhibited by reactions with the alkalies under similar conditions, the sodium-oxygen reactivity is expected to be smaller than the cesium-oxygen reactivity (27). Therefore, the oxygen and water contamination in our experiment (less than 1 ppm) should not significantly reduce the detectable sodium after a delay of several milliseconds.

The influence of the crystal orientation and surface target texture on the ablation pattern was studied for both Czochralski and float-zoned silicon in the counter gas atmosphere. Silicon samples, 1.1 by 0.7 by 0.05 cm with one face polished and the other face lapped, were ablated on each face with probe irradiances of about  $10^7$  to  $10^9 \text{ W/cm}^2$ . Czochralski samples <100> n-type (7 to 10  $\Omega\cdot\text{cm}$ ), <111> neutron transmutation doped (30  $\Omega\cdot\text{cm}$ ), and <110> p-type

(2.5 to 3.5  $\Omega \cdot \text{cm}$ ), and dislocation-free float-zoned samples,  $\langle 111 \rangle$  p-type (500 to 1200  $\Omega \cdot \text{cm}$ ),  $\langle 511 \rangle$  n-type (50 to 100  $\Omega \cdot \text{cm}$ ) were studied. No significant difference was found in ablation patterns generated on the polished or lapped face of the Czochralski samples. On the float-zoned samples, more surface redeposition was observed on the polished face than on the lapped face. Figure 5 shows the ablation pattern resulting on the float-zoned samples studied. A profilometer stylus used on the  $\langle 111 \rangle$  polished sample revealed a protruding rim developed around the cone-shaped crater with material redeposited on the surface. Clean regions on the target are indicative of material ejections close to the surface being captured by the protruding rim. On the lapped  $\langle 511 \rangle$  surface, no significant redeposition is observed around the bowl-shaped crater where a protruding rim is developed. Probe irradiances below  $10^7 \text{ W/cm}^2$  induce ablation patterns in silicon with no material redeposition outside the rim. The regularity of these low irradiance patterns permitted us to estimate the volume of evaporated material. Typically, for our LARIS observations, a  $10^7 \text{ W/cm}^2$  ablation irradiance was used on the silicon; each ablation pulse forms a crater measured by profilometer to be about  $10^{-8} \text{ cm}^3$  in volume, corresponding to  $5 \times 10^{14}$  silicon plus impurity atoms. The plume that expands in the buffer gas forms a gaseous sample with the number density of ablated species estimated to be about  $10^{14} \text{ cm}^{-3}$ .

Our demonstration of the intrinsically high sensitivity of the LARIS technique was performed on single crystal float-zoned silicon specimens with a low sodium contamination level which was determined by neutron activation analysis. The specimens were chemically cleaned and neutron-activated in clean polyethylene containers. After neutron irradiation, the specimens were

etched to remove any accidental surface contamination. The remaining sodium activity in the silicon bulk was below the neutron activation detection limit (0.3 ppb). The sodium LARIS signals from these specimens correspond on the average to about 500 sodium atoms in the analyzed volume of the plume. In a crude estimate which ignores a detailed treatment of the aforementioned complex phenomena associated with the laser ablation, we obtain an approximate sodium density of  $10^{11} \text{ cm}^{-3}$  in the specimens.

#### IV. Conclusions

LARIS is the first application of resonance ionization spectroscopy for trace analysis of solids. It may be developed into a powerful analytical technique since it has the capability of detecting a single atom in the ablated plume. We have demonstrated that it is sensitive enough to detect sodium concentrations less than  $10^{11} \text{ cm}^{-3}$  in a solid matrix. For absolute quantitative results, further research is required to correlate impurity measurements in the ablated material with impurity content in the solid. The main limitations associated with this technique are summarized as follows:

- a) It is destructive.
- b) Spatial resolution is determined by crater size (in the scale of several micrometers).
- c) Accurate depth profiling in homogeneous materials and thin films seems difficult to achieve in view of the nature of the ablation process.
- d) Chemical and physical matrix effects may introduce difficult-to-evaluate plume-to-solid composition correlation effects.

The high sensitivity achievable by this technique makes further research on characterizing the complex ablation process a worthwhile endeavor; with such research LARIS can be developed into a reliable analytical tool.

## References

1. S. M. Sze, *Physics of Semiconductor Devices*, p. 28, Wiley-Interscience, New York (1969).
2. G. S. Hurst, M. G. Payne, S. D. Kramer, and J. P. Young, *Rev. Mod. Phys.* 51, 767 (1979).
3. G. S. Hurst, M. H. Nayfeh, and J. P. Young, *Appl. Phys. Lett.* 30, 299 (1977), and *Phys. Rev. A15*, 2283 (1977).
4. S. D. Kramer, J. P. Young, G. S. Hurst, and M. G. Payne, *Opt. Comm.* 30, 47 (1979).
5. V. S. Letokhov, *Opt. and Laser Technol.* 10, 175 (1978).
6. G. I. Bekov, V. S. Letokhov, and V. I. Mishin, *JETP Lett.* 27, 47 (1978).
7. G. I. Bekov, V. S. Letokhov, O. I. Matveev, and V. I. Mishin, *Opt. Lett.* 3, 159 (1978).
8. M. Stupavsky and L. Krause, *Can. J. Phys.* 46, 2127 (1968).
9. The actual gas analysis shows 0.5 molar ppm oxygen and 0.5 molar ppm water. Dew point - 193°C.

10. R. W. P. Dever, A. Moljk, and S. C. Curran, *Nucl. Instr.* 1, 41 (1957).
11. G. F. Knoll, *Radiation Detection and Measurements*, Chapter 6, J. Wiley and Sons, New York (1979).
12. S. C. Curran, A. L. Cockroft, and J. Angus, *Phil. Mag.* 40, 929 (1949).
13. H. Genz, *Nucl. Instru. Meth.* 112, 83 (1973).
14. T. B. Lucatorto, T. J. McIllrath, S. Mayo, and H. W. Furumoto, *Appl. Optics* 19, 3178 (1980).
15. A. V. Smith, J. E. M. Goldsmith, D. E. Nitz, and S. J. Smith, *Phys. Rev. A22*, 577 (1980).
16. S. D. Rasberry, B. F. Scribner, and M. Margoshens, *Appl. Optics* 6, 81 and 87 (1967).
17. R. H. Scott and A. Strasheim, *Spectrochim. Acta* 25B, 311 (1970).
18. K. L. Morton, J. D. Nohe, and B. S. Madsen, *Appl. Spectroscopy* 27, 109 (1973).
19. D. E. Osten and E.H. Piepmeier, *Appl. Spectroscopy* 27, 165 (1973).
20. F. Brech and L. Cross, *Appl. Spectroscopy* 16, 59 (1962).

21. V. G. Mossotti, K. Laqua, and W. Hagenah, *Spectrochim. Acta* 23B, 197 (1967).
22. R. Measures and H. S. Kwong, *Appl. Optics* 18, 281 (1979).
23. F. Hillenkamp and E. Unsold, *Appl. Phys.* 8, 341 (1975).
24. D. W. Beekman, T. A. Calicott, S. D. Kramer, E. T. Arakawa, and G. S. Hurst, *Int. J. Mass Spectroscopy and Ion Phys.* 34, 89 (1980).
25. S. Ray, A. K. Pal, and A. K. Barua, *J. Phys. Soc. Japan* 42, 616 (1977).
26. V. I. Chigin, *Sov. Phys. Tech. Phys.* 20, 429 (1975).
27. J. Kleinberg, W. J. Argersinger, Jr., and E. Griswold, *Inorganic Chemistry*, Chapter 10, D. C. Heath and Co., Boston (1969).

## Figure Captions

Fig. 1. RIS experimental apparatus. (a) Instrumental setup. The arrows indicate gas flow through the counter.

1. proportional counter	6. mirror
2. electron suppression grid	7. laser probe splitter
3. field tubes	8. spectrograph-optical multichannel
4. probe collimation system	analyzer
5. 3:1 reducing telescope with spatial filter	9. silicon photodiode
	10. oven with sodium metal.

(b) A block diagram of the control electronics.

C clock	A amplifier
D variable delay	OSC memory oscilloscope
LT laser trigger	MCA multichannel analyzer
LH laser head	R silicon photodiode
PC proportional counter	

Fig. 2. RIS bipolar signal from sodium vapor in P-10 gas at 95 Torr and room temperature. Estimated sodium density in the gas is about 10 atoms/cm<sup>3</sup>. Vertical scale, 50 mV/div; horizontal scale, 2  $\mu$ s/div.

(a) Trace corresponds to both laser probes tuned to resonance wavelength,  
 $\lambda_1 = 589.99$  nm and  $\lambda_2 = 568.82$  nm.

(b) Trace corresponds to counter background when the  $\lambda_1$  probe is blocked.

Fig. 3. LARIS proportional counter cross section. The cylindrical cathode has apertures to admit the target and the ablation laser into the electric field region. The vapor sample is formed by the plume material in equilibrium with the counter gas. The RIS probes are directed parallel to the anode to irradiate the vapor sample.

Fig. 4. Laser-induced plasma in front of a silicon target in P-10 gas at 95 Torr. Laser irradiance is  $5 \times 10^9 \text{ W/cm}^2$ . The laser irradiates from the left, perpendicular to the target surface. A blue filter on an f/16 camera with 3000 ASA black and white film was used. The camera shutter remained open for several seconds while the ablation pulse (0.6- $\mu\text{s}$  duration) impinges on the target. The target height is 0.7 cm. The glowing region in front of the target is about 0.1  $\text{cm}^3$ .

Fig. 5. Ablation pattern on thick float-zoned silicon in P-10 gas at 95 Torr. Target size is 1.1 by 0.7 by 0.08 cm. Ten pulses (wavelength 592 nm, spectral width  $\pm 2 \text{ nm}$ , pulse irradiance  $2 \times 10^7 \text{ W/cm}^2$ ) were used to repetitively ablate on the same target spot with 2 min elapsed time between pulses.

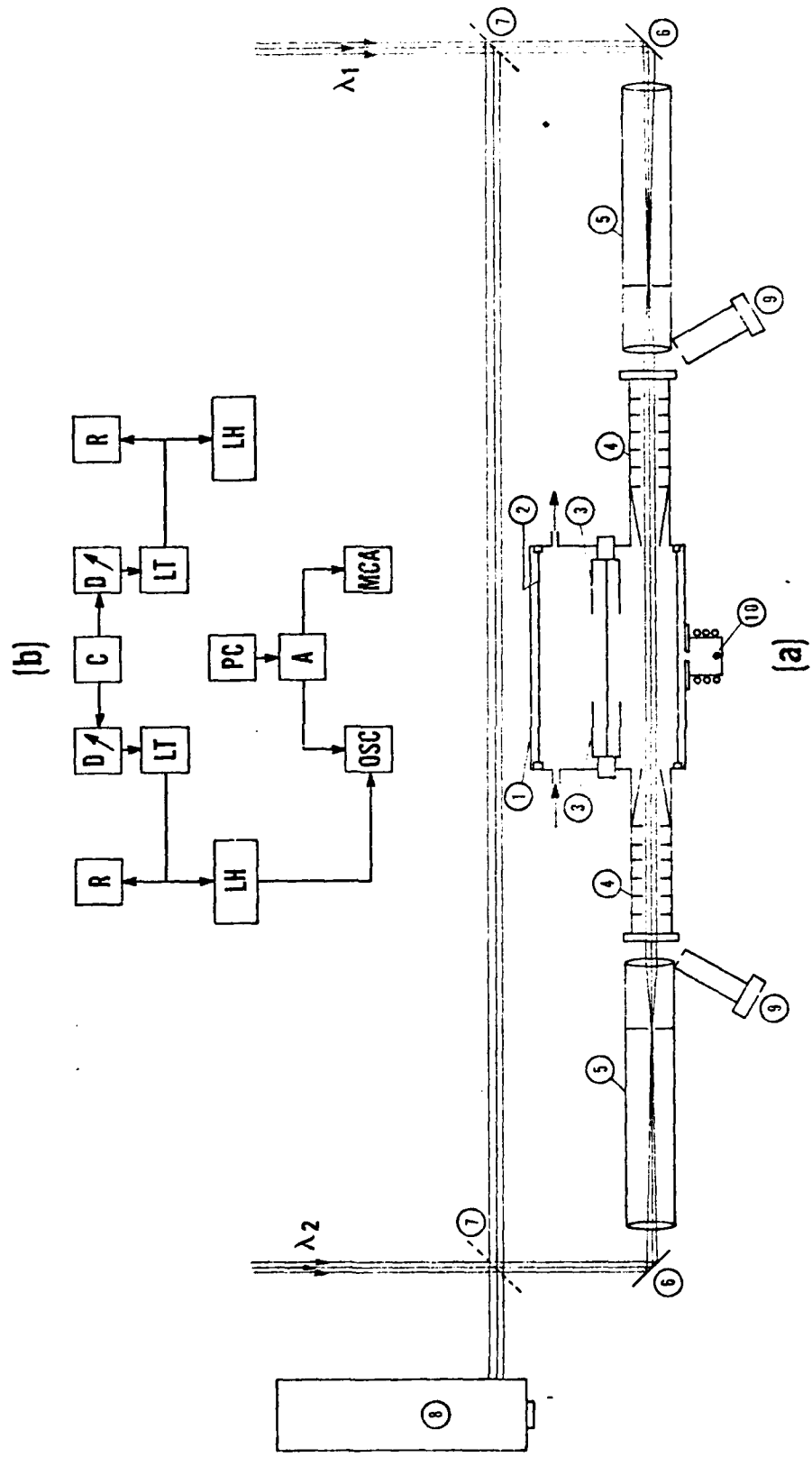
- (a) Mirror-polished silicon ( $<111>$  p-type,  $\rho \approx 500$  to  $1200 \Omega\text{-cm}$ ). Ejected material is redeposited around the cone-shaped developed crater. Clean regions on the surface are due to ejected material capture by protrusions formed around the crater. Crater diameter is about 50  $\mu\text{m}$ .
- (b) Lapped silicon (dislocation-free  $<511>$  n-type,  $\rho \approx 50$  to  $100 \Omega\text{-cm}$ ) showing surface roughness due to 5- $\mu\text{m}$  lapping material. The crater

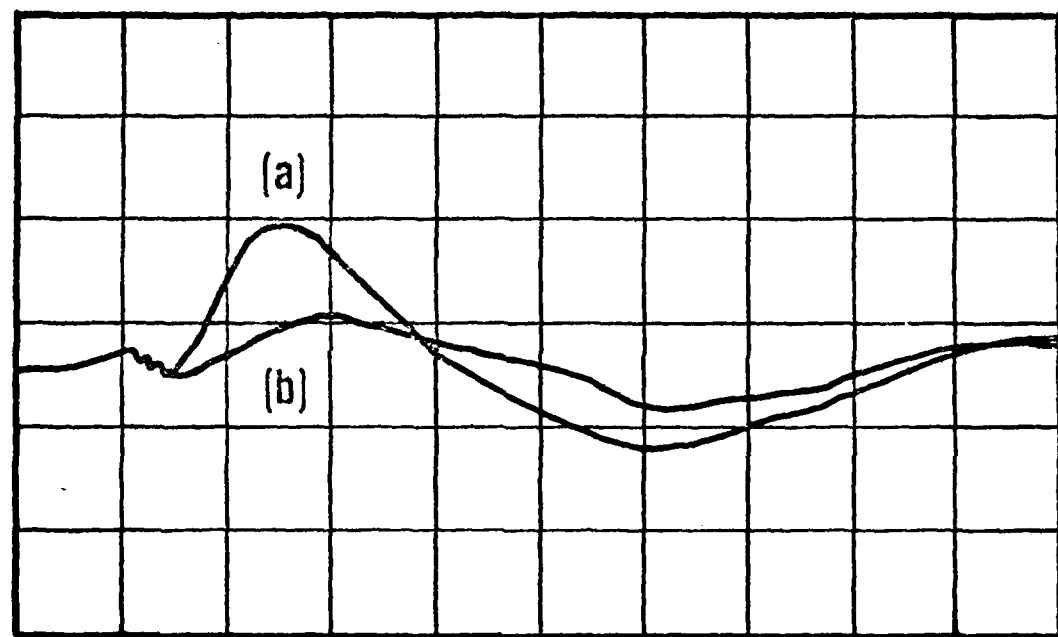
develops a bowl-shaped structure with a melted material rim. No significant target redeposition is observed. Crater diameter is about 100  $\mu\text{m}$ .

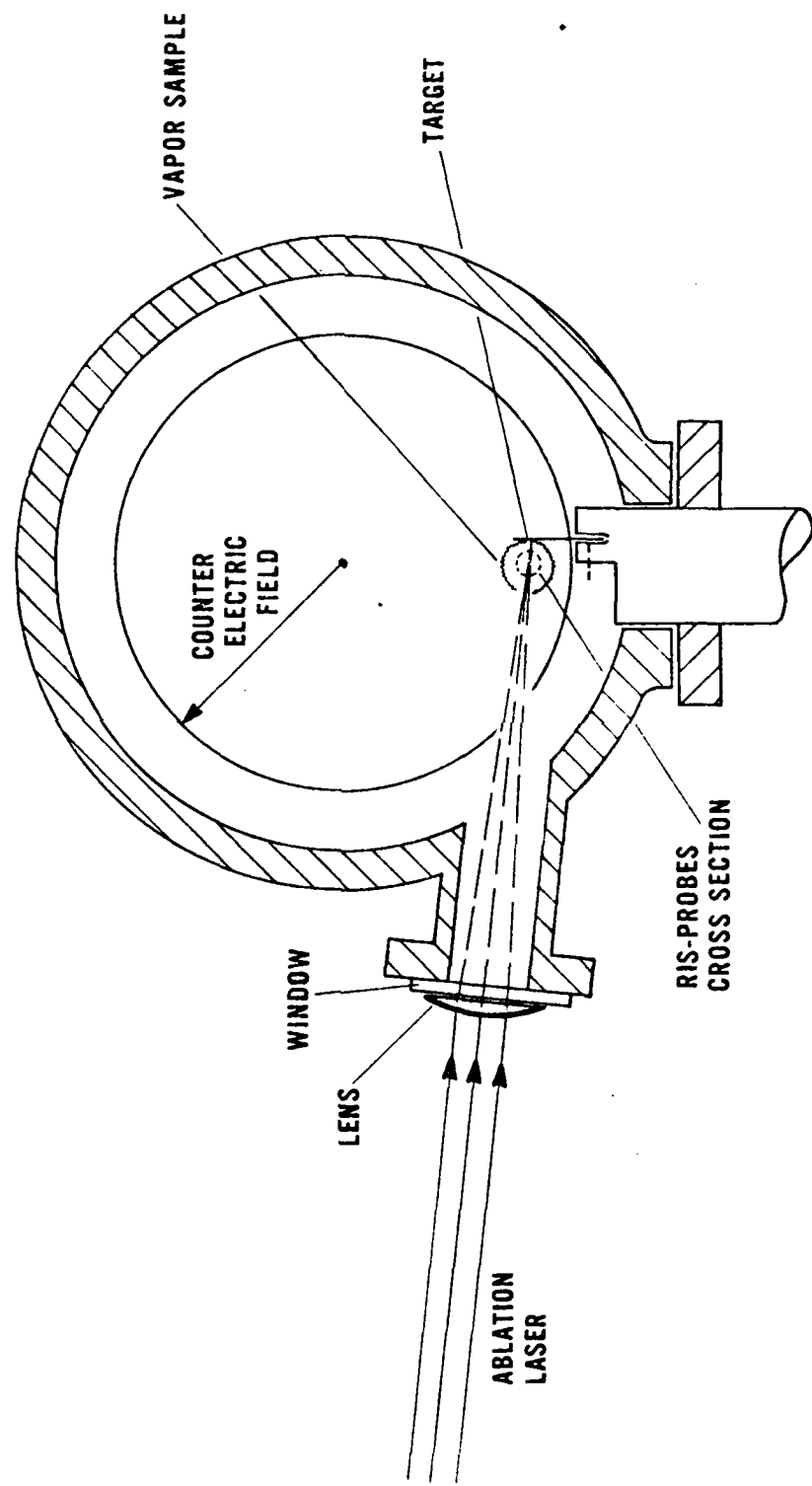
## Acknowledgments

We gratefully acknowledge J. K. Whittaker for his valuable help in designing the laser control electronics and reducing the electromagnetic pickup induced by the high-power lasers used for this work.

One of us (SM) is indebted to C. E. Dick for many enlightening discussions on nuclear detection techniques. R. M. Lindstrom provided neutron activation analysis results on the silicon samples used. D. Horowitz made available the ablation laser. We particularly thank G. S. Hurst and S. D. Kramer, Oak Ridge National Laboratory, for their kind attention in discussing single-atom detection schemes. This work was partially supported by the Office of Naval Research (NR 322-084). The stimulus and encouragement generously provided by L. R. Cooper to one of us (SM) is very much appreciated. Revision of the manuscript by G. P. Carver is very much appreciated.



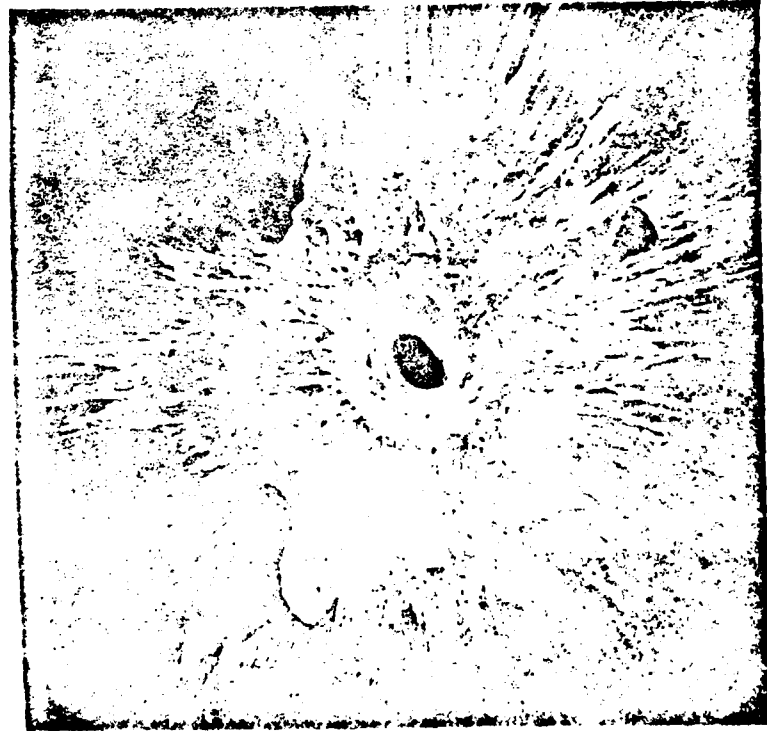








[b]



[a]